PHYSICAL REVIEW

LETTERS

VOLUME 57 17 NOVEMBER 1986 NUMBER 20

Quantum Nondemolition Detection of Optical Quadrature Amplitudes

M. D. Levenson, R. M. Shelby, M. Reid,[a] and D. F. Walls[a]

IBM Research, Almaden Research Center, San Jose, California 95120

(Received 25 August 1986)

In an optical fiber, nonlinear optical interactions couple the sideband modes of two strong pump waves at different frequencies just as required for a quantum nondemolition measurement. Experimental measurements demonstrate that 37% of the rms phase fluctuations of one wave are caused by the quantum amplitude fluctuations of the other.

PACS numbers: 03.65.Bz, 07.60.−j, 42.50.−p

The act of measurement of a quantum mechanical variable introduces uncertainty in subsequent measurements made on the same system. If only one variable is of interest, "quantum nondemolition" (QND) or "back-action evading" measurement schemes can be defined in which the uncertainty induced by the measurement feeds back into a decoupled conjugate variable, leaving the quantity of interest unchanged.[1-4]

We have implemented an optical quantum nondemolition detection scheme where "the variable of interest" is the quadrature corresponding to amplitude fluctuations of one wave and the "meter" or "readout" is the quadrature corresponding to phase fluctuations of a wave of a different frequency. The coupling between the QND variable and the meter is due to the optical Kerr effect in an optical fiber.[5,6] When all relevant four-wave mixing processes in the presence of two strong pump waves are included, the Hamiltonian for this coupling is of exactly the form required by simple QND measurement models.[4,7] Our results show a definite correlation between the QND measurement and the subsequent optical homodyne detection of the QND variable, but the signal-to-noise ratio is less than unity.

Six modes of the electromagnetic field must be considered in descriptions of our QND detector. Two modes—at the frequencies ω_x and ω_y—are strong classical pump waves with amplitudes E_x and E_y, respectively. Because of the nonlinear index of refraction, the slowly varying complex amplitudes of these modes propagate down the fiber according to

$$\partial E_x/\partial z = i(K_x + 2K_y)E_x, \qquad \partial E_y/\partial z = i(2K_x + K_y)E_y, \tag{1}$$

where the coupling constants are $K_j = (12\pi\omega_j/nc) f\chi^{(3)} \times |E_j|^2$ for $j = x,y$, $\chi^{(3)} = 5\times 10^{-15}$ cm^3/erg is the third-order nonlinear susceptibility, and f is a mode-overlap factor of order unity.[8]

The other four modes are shifted above or below one or the other pump wave by the same shift frequency δ. The quadrature operators for phase and amplitude modulation of the two pump beams at frequency δ are linear combinations of the creation and destruction operators for these four sideband modes.[9] It is convenient to introduce a local time variable $t = nz/c$ and to transform into the pump interaction picture. This is done by application of the unitary rotation operator $U = \exp(iRt)$, where

$$R = (c/n)[(K_x + 2K_y)(a_{x+}^\dagger a_{x+} + a_{x-}^\dagger a_{x-}) + (2K_x + K_y)(a_{y+}^\dagger a_{y+} + a_{y-}^\dagger a_{y-})] \tag{2}$$

and a_{x+}, a_{x-}, a_{y+}, and a_{y-}, are annihilation operators for the four sideband modes, with the + and − subscripts indicating the direction of frequency shift from the corresponding pump wave. For the wave E_x the (negative frequency) phase-modulation quadrature operator X_ϕ and the amplitude-modulation quadrature operator X_A are $X_\phi = -iU^\dagger(a_{x-} - a_{x+}^\dagger)U$ and $X_A = U^\dagger(a_{x-} + a_{x+}^\dagger)U$ while the corresponding operators for E_y are $Y_\phi = -iU^\dagger(a_{y-} - a_{y+}^\dagger)U$ and $Y_A = U^\dagger(a_{y-} + a_{y+}^\dagger)U$. The overall phase shift of the E_y field with respect to E_x is not relevant and has been set equal

to zero. The real and imaginary parts of X_A and Y_A comprise four independent (commuting) QND observables; similarly the real and imaginary parts of X_ϕ and Y_ϕ are four independent QND readouts.

The Hamiltonian for the nonlinear interactions of the sideband modes in an optical fiber is proportional to the time-averaged fourth power of the magnitude of the total electric field operator.[10] When written in the pump interaction picture, the sideband Hamiltonian takes the simple form

$$\mathcal{H}' = U^\dagger \mathcal{H} U - \hbar R$$
$$= (\hbar c/n)\{K_x X_A^\dagger X_A + K_y Y_A^\dagger Y_A + 2\gamma (K_x K_y)^{1/2}[X_A^\dagger Y_A + X_A Y_A^\dagger] + [\tilde{\Gamma}(X_A |E_x| + Y_A |E_y|) + \text{H.c.}]\}. \quad (3)$$

The operator $\tilde{\Gamma}$ describes phase noise produced by light-scattering processes in the fiber,[11] and γ is a polarization correlation factor. Fiber attenuation has been neglected. A key assumption in the derivation of Eq. (4) is that the frequency shifts $\omega_x - \omega_y$ and δ are such that all four-wave mixing processes involving the six indicated waves are phase matched but none that involve any additional waves are. In particular, new pump waves at $2\omega_x - \omega_y$ and $2\omega_y - \omega_x$ cannot be generated because of a large wave-vector mismatch. Such is the case whenever $(\omega_x - \omega_y)\delta < 10^4\ \text{GHz}^2 < (\omega_x - \omega_y)^2$.

The interaction term in this Hamiltonian is linear in each of the quadrature operators X_A and Y_A and is of the form required for a quantum nondemolition measurement which is also back-action evading.[4] The propagation equations for the quadrature amplitudes are

$$dX_A/dz = dY_A/dz = 0,$$
$$dX_\phi/dz = 2K_x X_A + 4\gamma (K_x K_y)^{1/2} Y_A + \tilde{\Gamma}|E_x|, \quad dY_\phi/dz = 2K_y Y_A + 4\gamma (K_x K_y)^{1/2} X_A + \tilde{\Gamma}|E_y|. \quad (4)$$

The quadratures at the output of the fiber are given by

$$X_A(z) = X_A(0), \quad Y_A(z) = Y_A(0), \quad (5a,b)$$
$$X_\phi(z) = X_\phi(0) + 2r_x X_A(0) + 4\gamma (r_x r_y)^{1/2} Y_A(0) + \tilde{\Gamma} z |E_x|, \quad (5c)$$
$$Y_\phi(z) = Y_\phi(0) + 2r_y Y_A(0) + 4\gamma (r_x r_y)^{1/2} X_A(0) + \tilde{\Gamma} z |E_y|, \quad (5d)$$

where $r_j = K_j z$ is the squeeze parameter.[8]

When neither r_x nor r_y is zero, the output phase quadratures $Y_\phi(z)$ and $X_\phi(z)$ contain information about the input amplitude quadratures $X_A(0)$ and $Y_A(0)$, respectively. These phase quadratures constitute meters in the QND sense. Measurement of one of these quantities allows inference of the amplitude quadrature to which it is coupled without perturbation of that amplitude quadrature. Hence, the measurement is back-action evading. In our experiment, the sideband fields at the fiber input are vacuum states.

Optical and rf heterodyne techniques allow measurement of the Hermitian real and imaginary parts of each of the quadratures. A local oscillator derived from one of the output pump waves and phase shifted by θ can beat with the sideband quadratures at the photodetector. The (negative frequency) operator for the δ Fourier component of the x photodetector current is

$$i_x(\theta) \propto \eta_x |\mathcal{E}_x^{LO}| \{[\cos\theta X_A(z) + \sin\theta X_\phi(z)] + (\eta_x^{-1} - 1)^{1/2} X_0\}, \quad (6)$$

where η_x is the detector quantum efficiency, X_0 is the quadrature operator for the vacuum state at phase angle θ, and a similar expression holds for the y modes. By this means, the X_ϕ quadrature amplitude can be detected and the $Y_A(0)$ input inferred with signal-to-noise ratio limited by the other terms in Eq. (5c). Thus, i_x is a QND meter for Y_A. It is, however, necessary to prove that this meter reads correctly by correlating it with Y_A.

In the present experiment, currents corresponding to the x and y photodetectors are amplified with gains g_x and g_y, the i_y signal is delayed by τ, and the two signals are combined: $i_{\text{tot}}(\delta) = g_x i_x(\theta) + \exp[i\delta\tau] g_y i_y(0)$. The delay of the δ Fourier component results in a phase shift $\delta\tau$. The local oscillator for the x detector is phase shifted by θ while that for the y detector is not shifted, i.e., Y_A is homodyne detected. The electrical noise power observed by an rf spectrum analyzer is proportional to $\frac{1}{2}\langle i_{\text{tot}}^\dagger(\delta) i_{\text{tot}}(\delta) + i_{\text{tot}}(\delta) i_{\text{tot}}^\dagger(\delta)\rangle$, which includes a term proportional to the desired correlation. The ratio of this noise power to that for a coherent state at the x detector with the same dc current is

$$V = 1 + Z^{-2} + \eta_x [2r_x \sin 2\theta + (2r_x^2 + \rho r_x)(1 - \cos 2\theta)] + 8\eta_x \gamma^2 r_x r_y (1 - \cos 2\theta) + 8Z^{-1}\gamma [\eta_x \eta_y r_x r_y]^{1/2} \sin\theta \cos(\delta\tau). \quad (7)$$

The parameter $Z = [g_x \eta_x^{1/2} |\mathcal{E}_x^{LO}| / g_y \eta_y^{1/2} |\mathcal{E}_y^{LO}|]$ accounts for differences in the gain between the two detectors.

Each of the five terms on the right-hand side of Eq. (7) has a unique interpretation. The first two represent the noise of the standard quantum limit on the x and y detectors, respectively. The third term results from the squeezing and excess phase noise due to the interactions of X_A and X_ϕ with each other and with the excitations responsible for the light

scattering, parametrized by the scattering strength ρ.[11] The fourth term is an excess phase noise for the x waves produced by the coupling to the quantum amplitude fluctuations of the y modes. This term is the mean square of the QND signal which measures the quadrature amplitude Y_A. The last term results from the nonclassical correlations between this QND signal and the photocurrent from the y detector which detects Y_A directly. Each of these quantities can be accessed experimentally and the results compared to Eq. (7).

The apparatus for the basic experiment appears in Fig. 1. A frequency-stabilized krypton-ion laser is made to operate on the two independent quantum-noise–limited transitions at 647 and 676 nm. The two wavelengths are separated by a prism to facilitate manipulation, recombined with another prism and coupled into a single-mode optical fiber. Not shown in the figure are cryogenic apparatus necessary to cool the fiber to 2 K to suppress phase noise and a phase modulator required to avoid stimulated Brillouin oscillation at low temperatures.[11] After the fiber, the two wavelengths are again split by another prism. The 647-nm beam is incident directly on an EG&G model FND-100 photodiode. The current fluctuations on this signal diode sense the amplitude quadrature Y_A. The 676-nm beam is reflected from a confocal interferometer[8] adjusted to shift the phase of the carrier wave by $\theta \approx -\pi/3$. The reflected beam is incident on a second, meter photodiode which produces current $i_x(\theta)$. The electrical signal currents from the two diodes are amplified, and one is delayed by a length of coaxial cable (delay time τ). The two signals are then combined on a hybrid junction which puts out the arithmetic sum of the currents into the spectrum analyzer. The average detector currents are recorded by use of digital voltmeters to calibrate the local oscillator intensities.

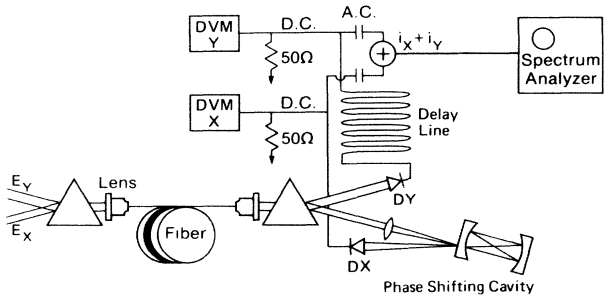

FIG. 1. The experimental apparatus. Strong pump waves at two different colors are combined by a prism, propagated through 114 m of single-mode optical fiber, and separated by a second prism. The Y wave is then incident on photodiode DY, which measures its amplitude-fluctuation noise, while the X wave encounters a phase-shifting interferometer. The DX photodiode produces current $i_x(\theta)$ which is sensitive to the phase quadrature fluctuation. The dc currents from both diodes are measured by digital voltmeters (DVM) and the ac noise currents are delayed and combined. The spectrum analyzer displays the electronic noise power in the combined signal.

In the basic experiment, signal and meter powers of 130 and 60 mW were coupled into the fiber and detected on the two photodiodes. The noise spectrum near the 56-MHz phase-noise minimum[11] appears as the solid circles of trace (a) in Fig. 2. The sinusoidal frequency dependence due to the correlations between Y_A and X_ϕ is readily apparent. Trace (b) shows a calibration trace taken by directing signal power equal to that in the former measurement into the y detector without propagating it through the fiber while maintaining exactly the same meter conditions. The constant level indicates the absence of correlations between the quantum-noise– limited signal detector current and the meter. The fact that the sinusoid of trace (a) falls below the uncorrelated noise level of trace (b) indicates that the fluctuations in $X_\phi(z)$ are correlated with the quantum fluctuations in $Y_A(0)$ through the nonlinear interaction in the fiber.

Other traces in Fig. 2 show the noise levels under other conditions. When only the meter beam is present in the fiber [trace (d)], the noise at the probe detector is above the quantum limit because of fiber-produced phase noise. When the Y wave also propagates through the fiber but is blocked from the y detector [trace (c)], the probe detector noise level rises further. This extra noise results from the nonlinear interaction between Y_A and X_ϕ

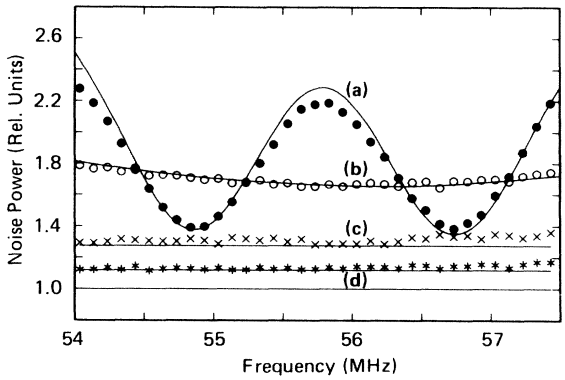

FIG. 2. The electronic noise power as a function of frequency δ. All traces are normalized to the standard quantum limit at the photodetector DX. The solid circles show the noise power for the experiment shown in Fig. 1 while the solid line in trace (a) is a fit by Eq. (8). The open circles and trace (b) show the experimental and predicted uncorrelated noise levels when the Y wave is incident directly on photodetector DY and not propagated through the fiber. The X wave continues to propagate through the fiber and is incident on detector DX with the same phase shift and power as in trace (a). The noise levels (c) and (d) were taken with no light on detector DY, but with and without the Y wave in the fiber, respectively. The difference between the two levels is the mean square of the QND signal. Again, the solid lines are predictions of Eq. (8). All the experimental points have an estimated 2% uncertainty, roughly equal to the radius of the solid circles.

and is given by the fourth term in Eq. (7).

The solid curve labeled as trace (a) in Fig. 2 is a fit of Eq. (7) to the experimental noise-power levels shown as solid circles. The parameters $\eta_x = 0.4$, $\eta_y = 0.64$, and $\theta = -\pi/3$ were measured in a subsidiary experiment. The squeeze parameters $r_x = 0.15$ and $r_y = 0.4$ as well as the phase noise ratio $\rho = 0.8$ could be estimated from data taken on this optical fiber previously.[11] The quantum noise on the y amplitude is Z^{-2} and is determined experimentally as the difference between traces (b) and (d). The remaining free parameter $\gamma = 0.6$ was adjusted to give the best fit. The predictions of this fit for the various other noise levels shown in Fig. 2 appear as solid lines.

In other experiments, the θ dependence of the noise levels and correlations predicted by Eq. (7) was verified. The coefficient of $\cos(\delta\tau)$ does vary as $\sin\theta$ as predicted, and the gain and local-oscillator amplitude dependence parametrized by Z also was as in Eq. (7). The amplitude-noise level of the y beam upon exiting from the fiber was within 2% of the standard quantum limit, verifying that the measurement is in fact back-action evading at least to the level of not adding fluctuations greater than the vacuum.

For the data shown in Fig. 2 approximately 37%, rms, of the measured fluctuations [trace (c)] of the detected X quadrature result from quantum fluctuations of Y_A. The remainder of the fluctuations [trace (d)] are due to quantum fluctuations and fiber-produced phase noise of the meter, corresponding to the first and third terms of Eq. (7). A QND measurement scheme seeks to detect the influence of a weak external force by making successive measurements of the signal. Our data predict a correlation coefficient of $(0.37)^2$ for two successive QND measurements, whereas perfect QND detection would yield 1. The corresponding noise level for a hypothetical external force is ~ 3 times the standard quantum limit. A QND detector with such a low signal-to-noise level may not have great practical utility, but the principle of QND detection has been verified.

This research was partly supported by the U.S. Office of Naval Research. The authors wish to thank S. H. Perlmutter and R. G. DeVoe for their assistance on this project, and to acknowledge stimulating conversations with Dr. Y. Yamamoto, Dr. N. Imoto, and Dr. C. M. Caves.

---

[a]Current address: University of Waikato, Hamilton, New Zealand.

[1]V. B. Braginsky, Y. I. Vorontsov, and K. S. Thorne, Science **209**, 547 (1980).

[2]C. M. Caves, K. S. Thorne, R. W. P. Drever, V. D. Sandberg, and M. Zimmermann, Rev. Mod. Phys. **57**, 341 (1980).

[3]W. G. Unruh, Phys. Rev. D **19**, 2888 (1979).

[4]C. M. Caves, in *Quantum Optics, Experimental Gravitation and Measurement Theory,* edited by P. Meystre and M. O. Scully (Plenum, New York, 1983), p. 567.

[5]V. B. Braginsky and S. P. Viatchanin, in Ref. 4, p. 627.

[6]G. J. Milburn and D. F. Walls, Phys. Rev. A **28**, 2065 (1983); N. Imoto, H. A. Haus, and Y. Yamamoto, Phys. Rev. A **32**, 2287 (1985).

[7]B. Yurke, J. Opt. Soc. Am. B **2**, 732 (1986); M. Hillery and M. O. Scully, in Ref. 4, p. 661.

[8]M. D. Levenson, R. M. Shelby, and S. H. Perlmutter, Opt. Lett. **10**, 514 (1985).

[9]C. M. Caves and B. L. Schumaker, Phys. Rev. A **31**, 3068, 3093 (1985).

[10]M. D. Levenson, in *Chemical Applications of Nonlinear Raman Spectroscopy,* edited by A. H. Harvey (Academic, New York, 1981).

[11]R. M. Shelby, M. D. Levenson, S. A. Perlmutter, R. G. DeVoe, and D. F. Walls, Phys. Rev. Lett. **57**, 691 (1986).